Physics Letters B 817 (2021) 136304

Contents lists available at ScienceDirect

Physics Letters B

www.elsevier.com/locate/physletb

Double polarisation observable $\mathbb{G}$ for single pion photoproduction from the proton

The CLAS Collaboration

N. Zachariou [a,*], D.P. Watts [a], J. McAndrew [b], L. Zana [c], M. Bashkanov [a], I.I. Strakovsky [d], R. Workman [d], A.V. Sarantsev [e,f], V. Nikonov [e,f,1], K.P. Adhikari [ak,2], S. Adhikari [r], M.J. Amaryan [ak], G. Angelini [d], W.R. Armstrong [g], H. Atac [aq], N.A. Baltzell [c], L. Barion [u], M. Battaglieri [c,w], I. Bedlinskiy [ag], F. Benmokhtar [o], A. Bianconi [at,z], A.S. Biselli [p], M. Bondi [w], F. Bossù [k], S. Boiarinov [c], W.J. Briscoe [d], W.K. Brooks [ar], D. Bulumulla [ak], D.S. Carman [c], J.C. Carvajal [r], A. Celentano [w], P. Chatagnon [aa], T. Chetry [af], G. Ciullo [u,q], B.A. Clary [m], P.L. Cole [ae,t], M. Contalbrigo [u], V. Crede [s], A. D'Angelo [x,an], N. Dashyan [ay], R. De Vita [w], M. Defurne [k], A. Deur [c], S. Diehl [al,m], C. Djalali [aj,ap], M. Dugger [h], R. Dupre [aa,g], H. Egiyan [c,ah], M. Ehrhart [g], A. El Alaoui [ar,g], L. El Fassi [af,g], L. Elouadrhiri [c], P. Eugenio [s], G. Fedotov [ap,ao,3], S. Fegan [a,au], A. Filippi [y], G. Gavalian [c,ak], G.P. Gilfoyle [am], F.X. Girod [c,k], D.I. Glazier [au], R.W. Gothe [ap], K.A. Griffioen [ax], L. Guo [r], K. Hafidi [g], H. Hakobyan [ar,ay], M. Hattawy [ak], D. Heddle [l,c], K. Hicks [aj], A. Hobart [aa], M. Holtrop [ah], Q. Huang [k], Y. Ilieva [ap], D.G. Ireland [au], E.L. Isupov [ao], D. Jenkins [av], H.S. Jo [ad], K. Joo [m], S. Joosten [g], D. Keller [aw,aj], A. Khanal [r], M. Khandaker [ai,4], A. Kim [m,ad], F.J. Klein [j], A. Kripko [al], V. Kubarovsky [c], L. Lanza [x], M. Leali [at,z], P. Lenisa [u,q], K. Livingston [au], I.J.D. MacGregor [au], D. Marchand [aa], L. Marsicano [w], V. Mascagna [as,z], B. McKinnon [au], Z.E. Meziani [g], T. Mineeva [ar,m], V. Mokeev [c,ao], A. Movsisyan [u], E. Munevar [d,5], C. Munoz Camacho [aa], P. Nadel-Turonski [c], K. Neupane [ap], A. Ni [ad], S. Niccolai [aa], G. Niculescu [ac], T.R. O'Connell [m], M. Osipenko [w], A.I. Ostrovidov [s], M. Paolone [aq,ap], L.L. Pappalardo [u,q], R. Paremuzyan [c,ay], E. Pasyuk [c], O. Pogorelko [ag], Y. Prok [ak,l,aw], D. Protopopescu [au], M. Ripani [w], B.G. Ritchie [h], J. Ritman [ab], A. Rizzo [x,an], G. Rosner [au], J. Rowley [aj], F. Sabatié [k], C. Salgado [ai], A. Schmidt [d], R.A. Schumacher [i], Y.G. Sharabian [c], U. Shrestha [aj], D. Sokhan [au], O. Soto [v], N. Sparveris [aq], S. Stepanyan [c], S. Strauch [ap], N. Tyler [ap], M. Ungaro [c,m], L. Venturelli [at,z], H. Voskanyan [ay], E. Voutier [aa], X. Wei [c], B. Yale [ax], J. Zhang [aw,ak], Z.W. Zhao [n,aw,ap]

[a] *University of York, York YO10 5DD, United Kingdom*
[b] *University of Edinburgh, Edinburgh EH9 3FD, United Kingdom*
[c] *Thomas Jefferson National Accelerator Facility, Newport News, VA 23606, United States of America*
[d] *The George Washington University, Washington, DC 20052, United States of America*
[e] *Helmholtz-Institut fuer Strahlen- und Kernphysik, Universität Bonn, 53115 Bonn, Germany*
[f] *National Research Centre "Kurchatov Institute", Petersburg Nuclear Physics Institute, Gatchina, 188300 Russia*
[g] *Argonne National Laboratory, Argonne, IL 60439, United States of America*
[h] *Arizona State University, Tempe, AZ 85287-1504, United States of America*
[i] *Carnegie Mellon University, Pittsburgh, PA 15213, United States of America*

* Corresponding author.
E-mail address: nicholas@jlab.org (N. Zachariou).

[1] Deceased.
[2] Current address: Hampton University, Hampton, VA 23668.
[3] Current address: Ohio University, Athens, Ohio 45701.
[4] Current address: Idaho State University, Pocatello, Idaho 83209.
[5] Current address: Universidad Distrital Francisco José de Caldas, 110311 Bogotá, Colombia.

https://doi.org/10.1016/j.physletb.2021.136304

[j] Catholic University of America, Washington, D.C. 20064, United States of America
[k] IRFU, CEA, Université Paris-Saclay, F-91191 Gif-sur-Yvette, France
[l] Christopher Newport University, Newport News, VA 23606, United States of America
[m] University of Connecticut, Storrs, CT 06269, United States of America
[n] Duke University, Durham, NC 27708-0305, United States of America
[o] Duquesne University, 600 Forbes Avenue, Pittsburgh, PA 15282, United States of America
[p] Fairfield University, Fairfield, CT 06824, United States of America
[q] Universita' di Ferrara, 44121 Ferrara, Italy
[r] Florida International University, Miami, FL 33199, United States of America
[s] Florida State University, Tallahassee, FL 32306, United States of America
[t] Idaho State University, Pocatello, ID 83209, United States of America
[u] INFN, Sezione di Ferrara, 44100 Ferrara, Italy
[v] INFN, Laboratori Nazionali di Frascati, 00044 Frascati, Italy
[w] INFN, Sezione di Genova, 16146 Genova, Italy
[x] INFN, Sezione di Roma Tor Vergata, 00133 Rome, Italy
[y] INFN, Sezione di Torino, 10125 Torino, Italy
[z] INFN, Sezione di Pavia, 27100 Pavia, Italy
[aa] Université Paris-Saclay, CNRS/IN2P3, IJCLab, 91405 Orsay, France
[ab] Institute fur Kernphysik (Juelich), Juelich, Germany
[ac] James Madison University, Harrisonburg, VA 22807, United States of America
[ad] Kyungpook National University, Daegu 41566, Republic of Korea
[ae] Lamar University, 4400 MLK Blvd, PO Box 10009, Beaumont, TX 77710, United States of America
[af] Mississippi State University, Mississippi State, MS 39762-5167, United States of America
[ag] National Research Centre Kurchatov Institute - ITEP, Moscow, 117259, Russia
[ah] University of New Hampshire, Durham, NH 03824-3568, United States of America
[ai] Norfolk State University, Norfolk, VA 23504, United States of America
[aj] Ohio University, Athens, OH 45701, United States of America
[ak] Old Dominion University, Norfolk, VA 23529, United States of America
[al] II Physikalisches Institut der Universitaet Giessen, 35392 Giessen, Germany
[am] University of Richmond, Richmond, VA 23173, United States of America
[an] Universita' di Roma Tor Vergata, 00133 Rome, Italy
[ao] Skobeltsyn Institute of Nuclear Physics, Lomonosov Moscow State University, 119234 Moscow, Russia
[ap] University of South Carolina, Columbia, SC 29208, United States of America
[aq] Temple University, Philadelphia, PA 19122, United States of America
[ar] Universidad Técnica Federico Santa María, Casilla 110-V, Valparaíso, Chile
[as] Università degli Studi dell'Insubria, 22100 Como, Italy
[at] Università degli Studi di Brescia, 25123 Brescia, Italy
[au] University of Glasgow, Glasgow G12 8QQ, United Kingdom
[av] Virginia Tech, Blacksburg, VA 24061-0435, United States of America
[aw] University of Virginia, Charlottesville, VA 22901, United States of America
[ax] College of William and Mary, Williamsburg, VA 23187-8795, United States of America
[ay] Yerevan Physics Institute, 375036 Yerevan, Armenia

ARTICLE INFO

Article history:
Received 5 November 2020
Received in revised form 5 April 2021
Accepted 15 April 2021
Available online 21 April 2021
Editor: M. Doser

ABSTRACT

We report measurements of π^+ and π^0 meson photoproduction from longitudinally spin-polarised protons by an energy tagged (0.73-2.3 GeV) and linearly polarised photon beam. A close to complete solid angle coverage for the reaction products was provided by the CEBAF Large Acceptance Spectrometer at Jefferson Laboratory. The double-polarisation observable $\mathbb{G}$ is extracted from Maximum Likelihood fits to the data, enabling the first accurate determination for the reaction $\vec{\gamma}\vec{p} \to \pi^+ n$, while also significantly extending the kinematic coverage for $\vec{\gamma}\vec{p} \to \pi^0 p$. This large data set provides an important constraint on the properties and spectrum of excited nucleon states decaying to $N\pi$ in the mass range from 1.4 to 2.2 GeV, as well as for background (non-resonant) photoproduction processes. The considerable improvement achieved in the description of the observable $\mathbb{G}$ within the SAID and Bonn-Gatchina approaches after implementation of our data, illustrates that the partial-wave analyses now significantly extend the knowledge on $N\pi$ photoproduction amplitudes at $W > 1.8$ GeV. A partial-wave analysis using the new high-precision data set has a large impact on the extracted properties of high-spin nucleon excited states.

1. Introduction

Hadrons are composite strongly-bound systems, whose fundamental properties derive from the internal dynamics between their constituents, quarks and gluons. As with any composite system the excitation spectrum has the potential to reveal details of the dynamics and interactions of their constituents, providing new insights into their structure and more generally, our detailed understanding of the nature and validity of non-perturbative Quantum ChromoDynamics (QCD). Phenomenological constituent quark models and, more recently, lattice QCD calculations [1,2] predict a rich spectrum of nucleon resonances, in contrast to the more limited spectrum of states that have (currently) been established experimentally [3]. The cause of this so-called "missing resonance" problem [4] has been a major focus for contemporary experimental hadron physics and on the theory side has led to alternative interpretations of nucleon structure [5–8] that reduce the number of predicted states. Several missing resonances were discovered in the multichannel analysis of exclusive meson photo- and hadroproduction with a decisive impact from the CLAS exclusive pho-

toproduction data [9]. In addition, another missing resonance was recently observed in the combined analysis of the $\pi^+\pi^- p$ photo- and electro-production data [10]. Furthermore, new results [11,12] on the nucleon resonance spectrum are consistent with the symmetry driven expectations, which predict many other missing resonances in the mass range above 2.0 GeV. These studies have demonstrated sensitivity of the $N\pi$ photoproduction data to the contributions from the missing resonances in this mass range.

The photoproduction of mesons from nucleon targets provides an excellent tool to better determine the excitation spectrum of the nucleon. The main complication for experimental studies of this spectrum arises from the strong overlap of many of the excited states. Due to their short lifetime the states have widths larger than their separation, a problem that is exacerbated for the more densely packed higher-lying states. With the exception of the lowest-lying states, clear resonance signals are not evident in cross section data. Meson photoproduction offers the possibility of measurement of an extensive set of polarisation observables, information that is mandatory for partial-wave analysis to disentangle the underlying spectrum.

The photoproduction of single pseudo-scalar mesons can be fully described using four complex reaction amplitudes [13]. To constrain these amplitudes without model assumptions in a "complete" measurement, we require a precise and kinematically complete determination of at least eight well-chosen observables [14, 15], involving single- and double-polarisation observables from combinations of polarised beam, target nucleon, as well as a determination of polarisation of the recoiling (final state) baryon at fixed energy and production angle. Each combination has a different sensitivity to the magnitudes and phases of these complex amplitudes. The number of measurements required to unambiguously extract multipole amplitudes, meaning a separation of the reaction into the contributions from different photon angular momenta and distinguishing their electric or magnetic character, is a related problem, as discussed in Ref. [16]. The different spins and parities of the excited states mean their contributions will be separated into different multipole amplitudes, which offers the possibility to determine resonance properties.

As part of a world programme to provide the necessary experimental data, single and double meson photoproduction experiments from polarised and unpolarised nucleon targets are of high scientific priority at the leading electromagnetic-beam facilities, with recent and ongoing programmes at CLAS at JLab, A2 at MAMI, CBELSA/TAPS and BGO-OD in Bonn, as well as LEPS at SPring-8 and ELPH in Japan.

The current data set for pion photoproduction from the proton is the most extensive of the various possible final states (see Ref. [17] for a recent summary), with quality data obtained for both final states (π^+ and π^0) in their unpolarised differential cross sections and polarised beam single polarisation observables. Measurements of single polarisation observables relating to the recoiling nucleon (P_y) have also been achieved with limited acceptance.

Precision measurements of double-polarisation observables in pion photoproduction are limited to the π^0 final state. Measurements of $\mathbb{G}$, $\mathbb{F}$ (linearly polarised photons on longitudinally and transversely polarised targets, respectively), and $\mathbb{E}$ (circularly polarised beam on a longitudinally polarised target) have been achieved [18–20]. Kinematically sparse measurements of C_x and C_z (circularly polarised photons with recoil polarisation) along with the single polarisation observable P_y (recoil polarisation) have been obtained with spectrometers [21,22] with only one large acceptance measurement obtained for C_x in π^0 photoproduction [23]. The situation for double polarisation measurements in the π^+ reaction is comparatively poor. Specifically, only the $\mathbb{E}$ observable [24] has been determined with large kinematical coverage and only one beam-target measurement of the $\mathbb{G}$ observable was performed in 1980 [25], with very limited statistical accuracy and kinematical coverage.

Here we report a new measurement of the double-polarisation observable $\mathbb{G}$ for $\vec{\gamma}\vec{p} \to \pi^0 p$ and $\vec{\gamma}\vec{p} \to \pi^+ n$. The experiment provides the first precise measurements up to 2.280 GeV centre-of-mass ($c.m.$) energy for the reaction $\vec{\gamma}\vec{p} \to \pi^+ n$, while significantly extending the kinematical coverage up to 2.265 GeV for the reaction $\vec{\gamma}\vec{p} \to \pi^0 p$. The simultaneous determination for both states provides new and powerful constraints on the isospin dependence of the amplitudes contributing to pion photoproduction.

2. Experimental setup

The experiment [26] was conducted in Hall B at the Thomas Jefferson National Accelerator Facility (JLab) utilising the CEBAF Large Acceptance Spectrometer (CLAS) [27] and the Tagger spectrometer [28]. CLAS, which was a toroidal magnetic-field analysing spectrometer, provided an efficient detection and reconstruction of charged tracks over a large fraction of the full solid angle (covering polar angles between 8° and 140° and about 83% of the azimuthal angle) using a variety of tracking, time-of-flight and calorimeter systems. The Tagger spectrometer, upstream of CLAS allowed the production of a linearly polarised photon beam using the coherent bremsstrahlung technique, with the produced photons being tagged by the detection of the post-bremsstrahlung electrons in a magnetic spectrometer. The determination of the degree of linear beam polarisation involved comparing the shape of the coherent bremsstrahlung spectrum to a spectrum obtained from theoretical bremsstrahlung calculations (details can be found in Refs. [29–31]). Specifically, the enhancement distributions, obtained from the ratio of the photon-energy distribution using the crystalline (diamond) radiator to the spectrum from an amorphous radiator, were used to constrain the relative contribution of the coherent and incoherent processes. This allowed a reliable determination of the energy-dependent degree of photon polarisation from fitting a theoretical spectrum produced by the analytical bremsstrahlung calculation [30].

Three incident electron beam energies (2.751, 3.539, and 4.599 GeV) and various settings of the orientation of the diamond radiator allowed the production of photons with a high degree of linear polarisation in the energy range between 0.7 and 2.3 GeV (achieved with 9 different configurations of beam energy and diamond radiator orientation). For each configuration, the direction of the linear photon polarisation was rotated between two orthogonal directions, which allowed a reliable determination of observables without detailed studies of the detector acceptance [32]. The degree of photon polarisation achieved was of the order of $p_\gamma = 0.70$ for both polarisation directions, with a total uncertainty of 6%.

The polarised photon beam impinged on the FRozen Spin polarised proton Target (FROST) [33]. This comprised frozen beads of butanol (C_4H_9OH) inside a 50 mm long target cup. The protons from the hydrogenic component of the butanol were dynamically polarised, by transfer of polarisation from polarised electrons using microwaves in a strong magnetic field. This procedure was carried out once every ~ 7 days during the run, with the polarisation of the target within CLAS maintained with a magnetised holding coil installed around the target cell. The direction of the target polarisation was routinely changed between two orientations: pointing along and against the beam direction, with its magnitude determined on a run-by-run basis using an NMR probe. An average target polarisation of $p_z = 0.82 \pm 0.05$ was achieved in this experiment. A carbon target was placed downstream of the butanol and was used to assess the contribution of events originating from the unpolarised nuclear components (C, O, ^{4}He, and ^{3}He) of the butanol target, which would "dilute" the signal.

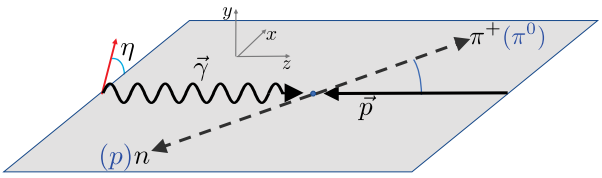

Fig. 1. The reaction $\vec{\gamma}\vec{p} \to \pi^+ n$ (and $\vec{\gamma}\vec{p} \to \pi^0 p$) in the *c.m.* frame. The *z*-axis is along the photon direction and the *y* axis is perpendicular to the reaction plane. The angle η is measured from the reaction plane defined by the photon and meson to the photon polarisation.

3. Polarisation observable $\mathbb{G}$

The polarised cross section for single pion photoproduction using a linearly polarised photon beam and a polarised compound target[6] for a specific kinematic bin in W and $\cos\theta_\pi^{c.m.}$ is given by [32]

$$\frac{d\sigma}{d\Omega}(W, \theta_\pi^{c.m.}, \eta) = \frac{d\sigma}{d\Omega}(W, \theta_\pi^{c.m.})\Big|_0 (1 - p_\gamma \Sigma^{eff} \cos(2\eta) + p_\gamma p_z^{eff} \mathbb{G} \sin(2\eta)), \quad (1)$$

where $\frac{d\sigma}{d\Omega}|_0$ is the unpolarised differential cross section, p_γ is the degree of linear polarisation of the photon beam and p_z^{eff} is the effective degree of target polarisation that takes into account contributions from unpolarised bound protons (see discussion in Sec. 4). The azimuthal angle, η, is the angle from the reaction plane (defined by the incident photon beam and the pion) to the vector polarisation of the photon, as indicated in Fig. 1. The effective beam-spin asymmetry Σ^{eff} and the double-polarisation observable $\mathbb{G}$ are functions of the centre-of-mass energy, W, and the polar production angle of the pion, $\theta_\pi^{c.m.}$, as indicated in Fig. 1.

A simultaneous determination of the double-polarisation observable $\mathbb{G}$ and the beam-spin asymmetry Σ^{eff} for each kinematic bin was performed by applying a Maximum Likelihood (ML) approach using the dependencies illustrated in Eq. (1).[7] The likelihood function for each event is given by

$$L_i = c\left[1 - p_{\gamma,i}\Sigma^{eff}\cos(2\eta_i) + p_{\gamma,i}p_{z,i}^{eff}\mathbb{G}\sin(2\eta_i)\right]A, \quad (2)$$

where c is a normalization coefficient and A is the detector acceptance.[8] The log-likelihood function that was maximised to obtain the observables of interest is given by

$$\log L = b + \sum_i \log\Big[1 - p_{\gamma,i}\Sigma^{eff}\cos(2\eta_i) + p_{\gamma,i}p_{z,i}^{eff}\mathbb{G}\sin(2\eta_i)\Big], \quad (3)$$

where the constant b is an observable-independent constant, which absorbs the normalization coefficient and detector acceptance. The summation (i) accounts for all events within a given kinematic bin. The extraction was carried out for ∼200 kinematic bins of W and $\cos\theta_\pi^{c.m.}$.

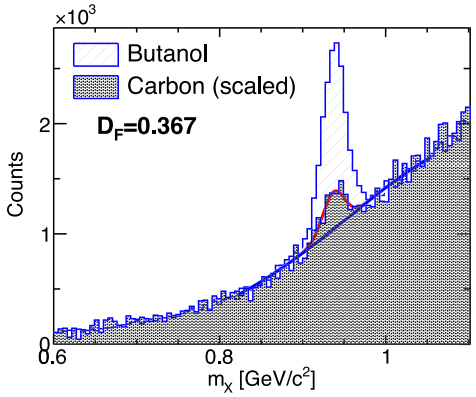

Fig. 2. Example of butanol missing-mass distribution overlaid with a scaled distribution from the carbon target for a specific kinematic bin ($W = 1740$ MeV, $\theta_\pi^{c.m.} = 80°$) for the reaction $\gamma p \to \pi^+ X$. The carbon and the sidebands of the butanol distributions were fitted simultaneously with a function used to determine the dilution factor, as described in the text. More representative plots and details on the procedure are provided in the supplementary documentation.

4. Data analysis

For each kinematic bin the event sample was analysed to remove the effects of backgrounds arising from unpolarised components of the target material and from background reaction processes. To achieve this, the missing-mass distributions of the reactions $\gamma p \to \pi^+ X$ and $\gamma p \to pX$ were obtained from the events originating from the butanol target, as well as from events originating from the carbon target.[9] Our approach assumes that polarisable protons contribute only to the missing-mass peak and bound unpolarised protons constitute the relatively broad background under the peak. The background thus dilutes the free-proton signal and its effect is determined by interpolating the sidebands from butanol data as well as utilising scaled carbon data for describing the background shape under the peak.

Fig. 2 shows the missing-mass distributions of $\gamma p \to \pi^+ X$ of events originating from the butanol (unshaded-blue histogram) target. The distribution exhibits the expected peak around the neutron mass, corresponding to events originating from the $\vec{\gamma}\vec{p} \to \pi^+ n$ reaction. However, this desired peak occurs on top of a broad background arising from reactions on (unpolarised) bound protons produced from the non-hydrogenic components of the polarised target. Also shown in the figure is the missing-mass distribution extracted from the carbon target for the same kinematic bin (shaded histogram). This distribution has been scaled by a factor α to fit the background in the butanol missing-mass distribution. It is seen that the data from the carbon target provides a good agreement with the shape of this unpolarised background, and was therefore used as the basis for establishing its relative contribution.[10] The blue line in Fig. 2 indicates the simultaneous fit performed on the carbon and the sidebands of the butanol distributions (outside 3σ of the free nucleon peak) that accounts for the bound nucleon contributions, whereas the red line includes con-

[6] In this case the polarised compound target consists of polarised free protons and unpolarised bound nucleons.

[7] The determined single polarisation observable Σ^{eff} reflects contributions from the free and the bound protons within the butanol target. The calculation of the contributions from free protons, therefore, requires a precise knowledge of Σ from bound protons, which could be obtained from nuclear targets. A more precise determination of Σ from free protons can be directly determined using an unpolarised hydrogen target (see for example Ref. [34]). Because of this, the beam-spin asymmetry Σ^{eff} is not reported.

[8] In the construction of the log-likelihood function, an approximation was made concerning the detector acceptance. Specifically, an acceptance that is largely independent of the kinematic variable η was assumed, which resulted in a normalization coefficient that is independent of the polarisation observables. This approximation significantly simplifies the extraction of the observables, but the assumption could potentially result in systematic biases. However, extensive simulation studies with the CLAS acceptance showed the effect of this to be negligible.

[9] The analysis focused on events where only the positively charged track was detected – either a proton or a pion – with the remaining neutral track reconstructed via the missing-mass technique.

[10] Note that a small fraction of the data originating from the carbon target produces a peak at the mass of the neutron, indicating a contribution from reactions on hydrogen. This was identified as arising from the formation of ice on the downstream target surface within the cryostat. Its effect was accounted for when calculating the dilution.

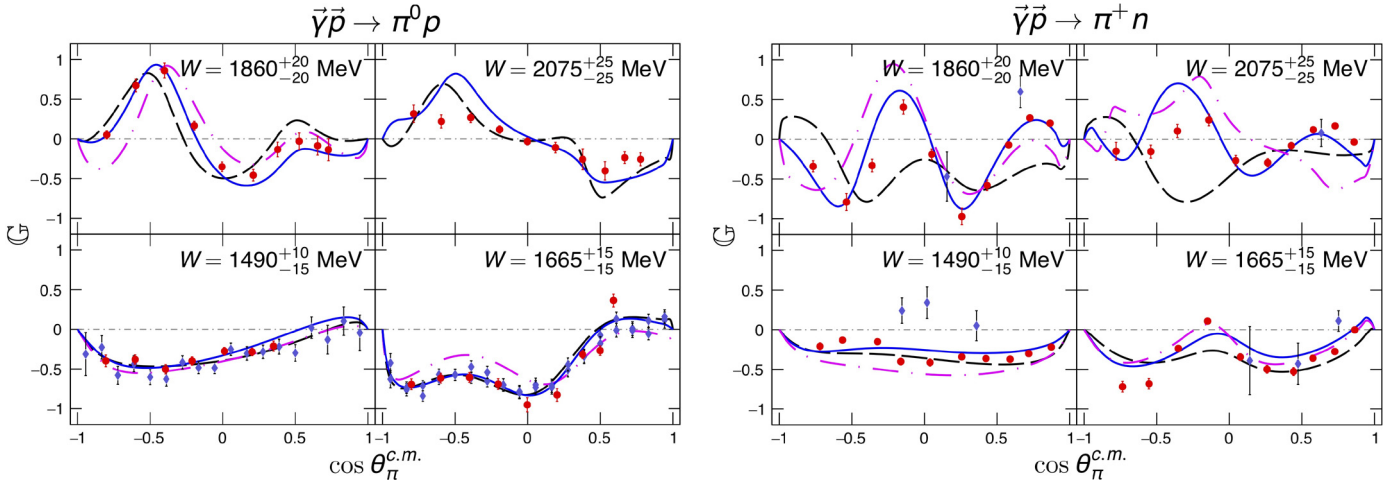

Fig. 3. A subset of the measured double-polarisation observable, $\mathbb{G}$, from this work for the reactions $\vec{\gamma}\vec{p} \to \pi^0 p$ (left) and $\vec{\gamma}\vec{p} \to \pi^+ n$ (right) as a function of the pion angle in the *c.m.* frame. The different panels denote bins in *c.m.* energy W. Experimental data from this work are shown with full red circles and from previous work with full blue diamonds. The error bars represent the combination of statistical and systematic uncertainties. The previous data for $\vec{\gamma}\vec{p} \to \pi^0 p$ came from the CBELSA Collaboration [18], and the previous data for $\vec{\gamma}\vec{p} \to \pi^+ n$ came from the NINA facility [25]. The blue solid curves correspond to predictions by SAID (MA19) [35], the black dashed to predictions by Bonn-Gatchina [11], and the magenta dash-dotted curves to predictions by MAID [36].

tributions from hydrogen contamination within the carbon target. More details are provided in the online supplementary material.

The unpolarised contributions result in a dilution of the target polarisation p_z by a factor of D_F: $p_z^{eff} = p_z D_F$. The dilution factor D_F was determined using the scaled-carbon missing-mass and butanol missing-mass distributions to establish the number of pion events that originated from bound nucleons, N_{bnd}. From this the dilution factor was calculated as

$$D_F = 1 - \frac{N_{bnd}}{N_T}\,, \tag{4}$$

where N_T is the number of events from butanol data under the missing-neutron peak for the reaction $\gamma p \to \pi^+ X$ or the missing-pion peak for the reaction $\gamma p \to pX$. More details on the dilution factor determination and how the fits were obtained are provided in the supplementary documentation. The range of integration in the missing mass was taken as $\pm 3\sigma$, where σ is the standard deviation of the peak. In the analysis the dilution factor (obtained on a bin-by-bin basis) was on average 0.40.

The statistical uncertainty of $\mathbb{G}$ was determined combining the uncertainties from the ML technique and the statistical uncertainty associated with the dilution factor determination, which was of the order of 2%. The relative systematic uncertainty was dominated by uncertainties associated with the determination of the photon and target polarisations, each of which contribute a 6% uncertainty. An extensive list of systematic sources was studied, including particle identification, reaction reconstruction, dilution factor determination and acceptance effects, with a total absolute contribution of 0.017 for $\vec{\gamma}\vec{p} \to \pi^+ n$ and 0.026 for $\vec{\gamma}\vec{p} \to \pi^0 p$, which was added to the relative systematic uncertainties. For a complete list of systematic uncertainties and further details on the analysis procedure see the supplementary documentation online.

5. Results and discussion

The results for the double-polarisation observable $\mathbb{G}$ as a function of the pion polar production angle in the *c.m.* frame for selected W bins for both reactions are shown in Fig. 3 (left panels for $\vec{\gamma}\vec{p} \to \pi^0 p$ and right panels for $\vec{\gamma}\vec{p} \to \pi^+ n$). The curves representing the previous phenomenological solutions from SAID MA19 [35] (blue solid), Bonn-Gatchina [11] (black dashed) and MAID [36] (magenta dashed-dotted) are also illustrated.

The agreement between the CLAS and previously published data for the reaction $\vec{\gamma}\vec{p} \to \pi^0 p$ is well within statistical uncertainties (see left panels of Fig. 3), providing further confidence in the analysis procedure. Previously published data provide measurements for the full angular coverage with *c.m.* energies up to $W = 1820$ MeV.[11] At low *c.m.* energies, W, forward-going pions correspond to protons with energies below the CLAS acceptance and thus the angular coverage for the CLAS data is more limited. However, the current analysis significantly extends the energy coverage for $\vec{\gamma}\vec{p} \to \pi^0 p$ from $W = 1425$ MeV to $W = 2265$ MeV. Partial-wave analysis solutions, which only included previously published data, describe well the angular dependence of $\mathbb{G}$ up to $W = 1740$ MeV. At higher energies, both partial-wave analysis solutions predict the features in the angular dependence of $\mathbb{G}$ for $\vec{\gamma}\vec{p} \to \pi^0 p$, but do not describe well their magnitude.

The agreement between the CLAS and previously published data for the reaction $\vec{\gamma}\vec{p} \to \pi^+ n$, is also well within statistical uncertainties for all but one kinematic bin. The previous measurements from the NINA facility for the kinematic bin with *c.m.* energies $W = 1490$ MeV indicate a positive value of $\mathbb{G}$, where the new precise measurement from CLAS shows negatives values at the same pion production angles (see right panels in Fig. 3). The phenomenological curves indicating the previous solutions from SAID, Bonn-Gatchina, and MAID do predict the rich features seen in the angular dependence of $\mathbb{G}$ but fail to describe the magnitude, in particular at higher W bins and backward angles.

The new data on $\mathbb{G}$ have a significant effect on the amplitudes especially at *c.m.* energies above 1800 MeV, where no previous precise $\mathbb{G}$ data on either reaction exists. As was found in the study of Ref. [11], recent high-precision polarisation data have resulted in a closer agreement of multipole analyses, particularly at intermediate energies. In this regard, the comparison of fits to $\pi^+ n$ $\mathbb{G}$ data in Fig. 3 at 1490 MeV is interesting. The Bonn-Gatchina, SAID, and much older MAID solutions all agree with the present measurements even though the existing data from the NINA facility, of much lower precision, suggested an opposite sign. At the highest energies large differences in the predictions are apparent. However, this can occur without large differences at the multipole level, resulting instead from delicate cancellations.

[11] Data from CLAS were binned in larger W bins than the results from CBELSA and thus the two sets of points in specific panels.

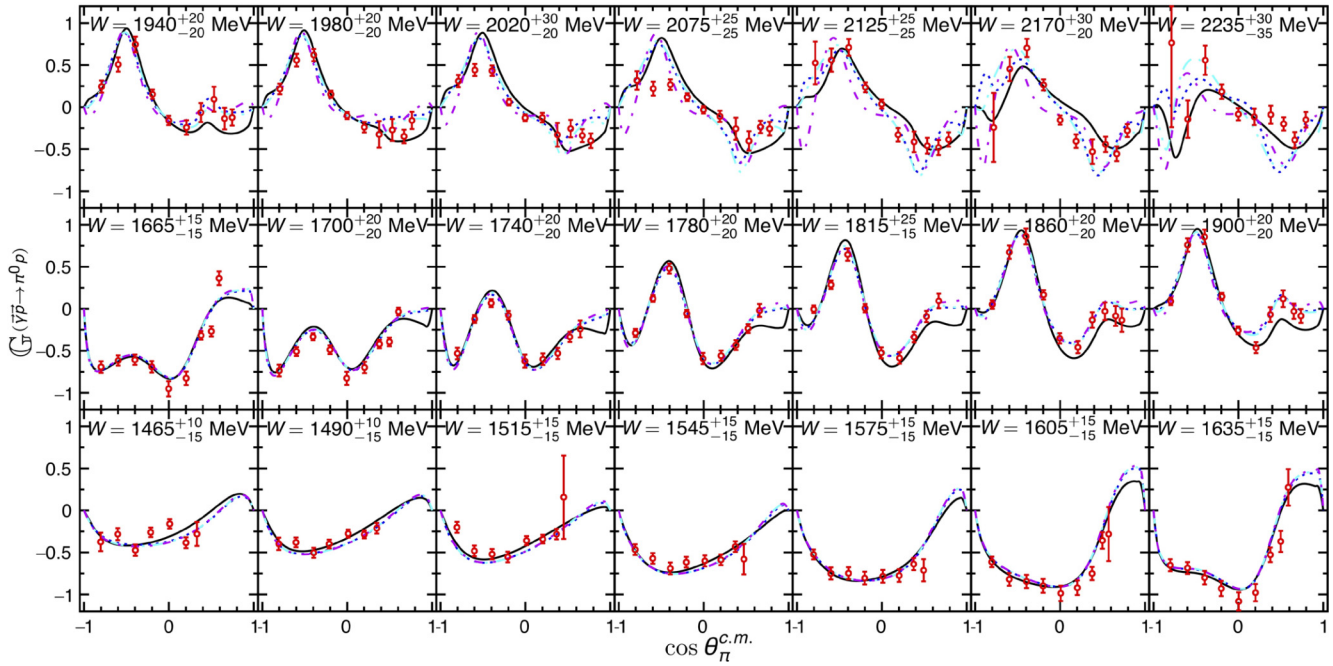

Fig. 4. Double-polarisation observable, $\mathbb{G}$, for the reaction $\vec{\gamma}\vec{p}\to\pi^0 p$ as a function of the pion angle in the *c.m.* frame. The different panels denote bins in *c.m.* energy W, with the mean values and widths indicated in each plot. The experimental data from this work are shown by the red circle with error bars denoting the total uncertainties. The new SAID ZA19 description (black solid curve), and the Bonn-Gatchina solutions (solution 1 - blue dotted, solution 3 cyan dash dotted-dotted, and solution 4 magenta dash-dotted; see text for details on solutions) are also indicated in the panels (solution 2 not shown). Differences between the four Bonn-Gatchina solutions are only evident at higher W.

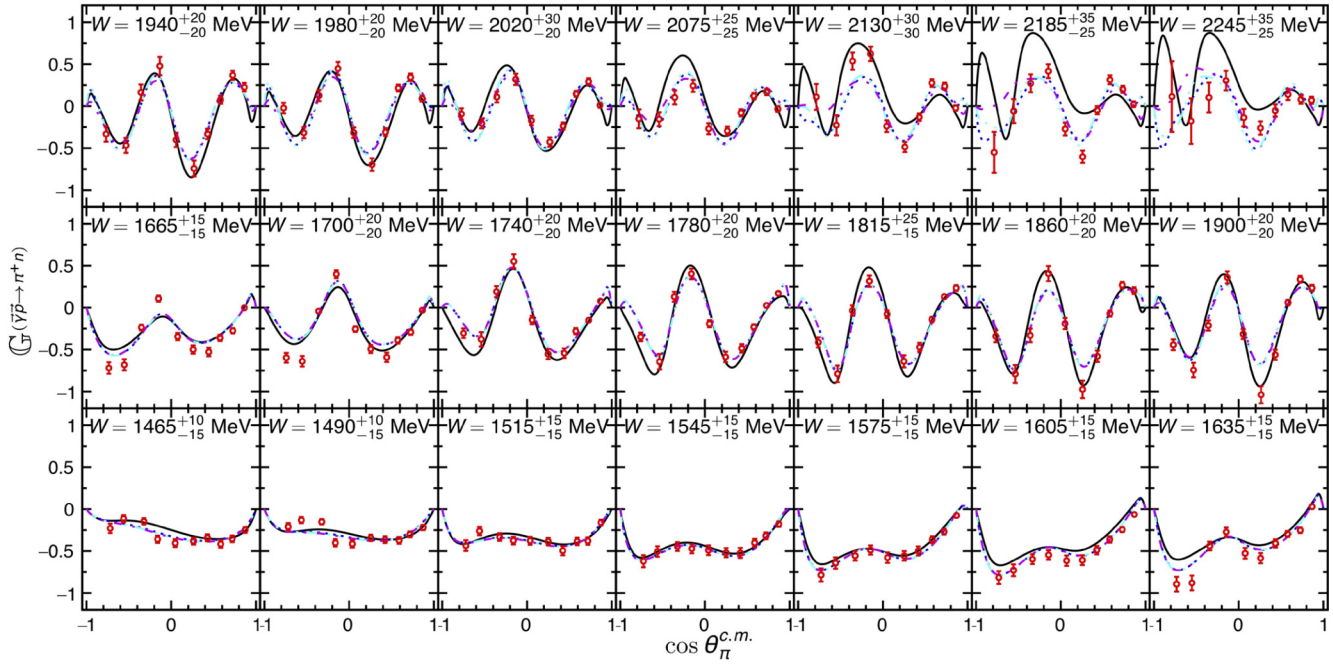

Fig. 5. Double-polarisation observable, $\mathbb{G}$, for the reaction $\vec{\gamma}\vec{p}\to\pi^+ n$ as a function of the pion production angle in the *c.m.* frame. The different panels denote bins in *c.m.* energy W, with the mean values and widths indicated in each plot. The experimental data from this work are shown by the red circle with error bars denoting the total uncertainties. The new SAID ZA19 description (black solid curve), and the Bonn-Gatchina solutions (solution 1 - blue dotted, solution 3 - cyan dash dotted-dotted, and solution 4 - magenta dashed dotted; see text for details on solutions) are also indicated in the panels (solution 2 not shown). Differences between the four Bonn-Gatchina solutions are only evident at higher W.

Figs. 4 and 5 show the CLAS results from this work for the reactions $\vec{\gamma}\vec{p}\to\pi^0 p$ and $\vec{\gamma}\vec{p}\to\pi^+ n$, respectively, illustrating the new solutions from SAID and Bonn-Gatchina.[12] This analysis provides the first precise result on the double-polarisation observable $\mathbb{G}$ for the reaction $\vec{\gamma}\vec{p}\to\pi^+ n$ for the full angular coverage between *c.m.* energies $W = 1425$ MeV and $W = 2280$ MeV (see supplementary documentation for the lowest energy bin), which significantly enhances the database for this reaction. The new phenomenological solution from SAID (ZA19) is indicated with black

[12] The results for the lowest energy bin for both reactions are shown in the supplementary documentation.

solid curves and three solutions from the Bonn-Gatchina group are shown with the blue dotted, cyan dashed dotted-dotted and magenta dash dotted curves. The results were fitted taking into consideration the fully-correlated scale uncertainties, which only influences the magnitude but not the shape of the curves, as well as the point-by-point absolute systematic uncertainties (see supplementary documentation for further details).

In terms of the Bonn-Gatchina approach, the description with the solution from Refs. [11,12] failed to describe the new data on charged pion photoproduction in the mass region above 1800 MeV (the total χ^2 was found to be 64.6 per data point). The solution presented in Ref. [37], which described well the helicity asymmetry data measured by the CLAS and CBELSA Collaborations, gave a much better description of the data although it was still far from being satisfactory. The refit of all data allowed us to obtain a good description of these new $\mathbb{G}$ data. We refer to this as Solution 1 and is indicated by the blue dotted curves in Figs. 4 and 5. Contributions from high-spin states were investigated by removing such states and refitting the data set. Contributions from the $\Delta(2400)9/2^-$ state (solution 2, not shown in figures) was first established. In this fit, the χ^2 for the description of other pion photoproduction data increased slightly, however, the description of the new polarisation data for the $\vec{\gamma}\vec{p} \to \pi^+ n$ reaction did not change, and a slight improvement was observed in the description of $\mathbb{G}$ for the reaction $\vec{\gamma}\vec{p} \to \pi^0 p$. This indicates that this state does not play a direct role in the description of the new data, although it provides better consistency between the old and new data. In solution 3 (cyan dash dotted-dotted curves), the $N(2220)9/2^+$ state was also removed (in addition to the $\Delta(2400)9/2^-$). This solution resulted in a small increase of the reduced χ^2 from 2.10 to 2.13. From Figs. 4 and 5 it is evident that the $N(2220)9/2^+$ state has some influence on the high-energy tail of the $\mathbb{G}$ distribution, however, both of the 9/2 states do not contribute notably to the description of the data. Finally, solution 4 (magenta dashed dotted curves) was obtained by removing the $\Delta(2200)7/2^-$ in addition to the $\Delta(2400)9/2^-$. The reduced χ^2 for $\mathbb{G}$ for the reaction $\vec{\gamma}\vec{p} \to \pi^+ n$ increased from 2.10 to 2.32 and for reaction $\vec{\gamma}\vec{p} \to \pi^0 p$ increased from 2.10 to 2.74. This is a notable effect since it affects only a few high-energy bins and we can conclude that contributions from the $\Delta(2200)7/2^-$ are much stronger.

The most notable change in solution 4 was connected with re-determination of the properties of the $N(2190)7/2^-$ state. In the main solution 1, the mass of this state was found to be 2120±20 MeV, which is 30 MeV lower than in the analysis [12], with a width of 380 ± 25 MeV, which is larger by 15%. Although the elastic residue and its phase practically did not change, the $A_{1/2}$ helicity coupling in the pole was found to be -40 ± 8 [GeV$^{-1/2}10^{-3}$] compared to -68 ± 5 [GeV$^{-1/2}10^{-3}$] in Ref. [12], with phase of $15^\circ \pm 10^\circ$ compared to $10^\circ \pm 12^\circ$ in Ref. [12]. The $A_{3/2}$ helicity coupling increased from 25 ± 10 [GeV$^{-1/2}10^{-3}$] [12] and was optimized at 67 ± 15 [GeV$^{-1/2}10^{-3}$], with a phase of $0^\circ \pm 15^\circ$ compared to $22^\circ \pm 10^\circ$ in Ref. [12]. The new values are very close to those obtained in the analysis [38]. This analysis clearly indicates that the contribution of both states ($N(2190)7/2^-$ and $\Delta(2200)7/2^-$) is important for the description of the current data. The $\Delta(2200)7/2^-$ is an important state for checking for chiral restoration at high energy. In the case of chiral restoration its mass should be close to the mass of the $\Delta(1950)7/2^+$ state, however it appeared to be 200-250 MeV higher. In the present analysis the pole position was found to be 2120 ± 30 MeV with a width of 430 ± 30 MeV. This indicates that the present solution finds a notably broader state than the solution presented in Ref. [37]. The $A_{1/2}$ helicity coupling at the pole was found to be 100 ± 15 [GeV$^{-1/2}10^{-3}$] with phase $-20^\circ \pm 20^\circ$ and $A_{3/2}$ at 25 ± 10 [GeV$^{-1/2}10^{-3}$] with phase $-10^\circ \pm 20^\circ$, which presents an increase by a factor of 1.6 for the helicity coupling for the $A_{1/2}$, whereas the helicity coupling $A_{3/2}$ changed its sign. This sign could not be defined on the basis of the other observables and the measurement of the $\mathbb{G}$ observable provided the critical information needed to establish it.

Interestingly, the $N(2190)7/2^-$ pole position from Bonn-Gatchina has moved into closer agreement with the SAID determination [39]. The helicity amplitudes for this state are now also in closer agreement with those found in Ref. [38]. These two $7/2^-$ states are found in both the Bonn-Gatchina and Jülich-Bonn analyses [40], but the Δ state is absent from the SAID fit. From the SAID analysis, the $N(2190)7/2^-$ partial waves have remained fairly stable with a tuning of lower-spin states, resulting in an improved fit to data. It should be noted that the SAID fits, by construction, cannot include states undetected in their analyses of pion-nucleon scattering data.

6. Summary

We present the first precise measurement of the double-polarisation beam–target observable $\mathbb{G}$, employing a linearly polarised photon beam and a spin-polarised target, for $\vec{\gamma}\vec{p} \to \pi^+ n$ up to *c.m.* energies $W = 2280$ MeV, while significantly extending the available kinematic coverage for $\vec{\gamma}\vec{p} \to \pi^0 p$ up to *c.m.* energies $W = 2265$ MeV. The new $\mathbb{G}$ data are an important addition to the world database and have a large effect on the determined amplitudes, especially at *c.m.* energies above 1800 MeV. Furthermore, the unprecedented quantity of the data impose tight constraints on partial-wave analyses, particularly for high-L multipoles and at high *c.m.* energies, where missing resonances are expected to exist. The new data were fit in the frameworks of the SAID and Bonn-Gatchina partial-wave analyses, which resulted in tightly constrained amplitudes. The Bonn-Gatchina analysis has illustrated the importance of the $N(2190)7/2^-$ and $\Delta(2200)7/2^-$ states in describing the data, while further constraining their masses and widths, whereas the SAID analysis allowed us to fine tune the lower-spin states. A more detailed analysis in the SAID and Bonn-Gatchina frameworks will be presented in a later paper.

Declaration of competing interest

The authors declare that they have no known competing financial interests or personal relationships that could have appeared to influence the work reported in this paper.

Acknowledgements

This work has been supported by the U. K. Science and Technology Facilities Council (ST/P004385/2, ST/T002077/1, and ST/L00478X/2) grants, as well as by the Department of Energy (DE-SC0016582) grant. We also acknowledge the outstanding efforts of the staff of the Accelerator and Physics Divisions at Jefferson Lab that made this experiment possible. This work was supported in part by the U.S. Department of Energy, Office of Science, Office of Nuclear Physics under Awards No. DE–SC0016583 and DE–SC0016582 and Contract No. DE–AC05–06OR23177. Further support was provided by the U.S. National Science Foundation, the Italian Istituto Nazionale di Fisica Nucleare, the Chilean Comisión Nacional de Investigación Científica y Tecnológica (CONICYT), the French Centre National de la Recherche Scientifique, the French Commissariat à l'Énergie Atomique, and the National Research Foundation of Korea.

Appendix A. Supplementary material

Supplementary material related to this article can be found online at https://doi.org/10.1016/j.physletb.2021.136304.

References

[1] V. Crede, W. Roberts, Rep. Prog. Phys. 76 (2013) 076301.
[2] E. Klempt, J.-M. Richard, Rev. Mod. Phys. 82 (2010) 1095.
[3] P. Zyla, et al., Particle Data Group, Prog. Theor. Exp. Phys. 2020 (2020) 083C01.
[4] R. Koniuk, N. Isgur, Phys. Rev. Lett. 44 (1980) 845.
[5] M. Anselmino, E. Predazzi, S. Ekelin, S. Fredriksson, D. Lichtenberg, Rev. Mod. Phys. 65 (1993) 1199.
[6] S.J. Brodsky, Eur. Phys. J. A 31 (2007) 638.
[7] E. Kolomeitsev, M. Lutz, Phys. Lett. B 585 (2004) 243.
[8] S. Afonin, Int. J. Mod. Phys. A 22 (2007) 4537.
[9] A.V. Anisovich, et al., Phys. Rev. Lett. 119 (2017) 062004.
[10] V. Mokeev, et al., Phys. Lett. B 805 (2020) 135457.
[11] A. Anisovich, et al., Eur. Phys. J. A 52 (2016) 284.
[12] V. Sokhoyan, et al., The CBELSA/TAPS Collaboration, Eur. Phys. J. A 51 (2015) 95.
[13] I.S. Barker, A. Donnachie, J.K. Storrow, Nucl. Phys. B 79 (1974) 431.
[14] G. Keaton, R. Workman, Phys. Rev. C 54 (1996) 1437.
[15] W.-T. Chiang, F. Tabakin, Phys. Rev. C 55 (1997) 2054.
[16] R. Workman, L. Tiator, Y. Wunderlich, M. Doering, H. Haberzettl, Phys. Rev. C 95 (2017) 015206.
[17] D.G. Ireland, E. Pasyuk, I. Strakovsky, Prog. Part. Nucl. Phys. 111 (2020) 103752.
[18] A. Thiel, et al., CBELSA/TAPS Collaboration, Phys. Rev. Lett. 109 (2012) 102001.
[19] J.R. Annand, et al., A2 Collaboration at MAMI, Phys. Rev. C 93 (2016) 055209.
[20] M. Gottschall, et al., CBELSA/TAPS Collaboration, Phys. Rev. Lett. 112 (2014) 012003.
[21] K. Wijesooriya, et al., Phys. Rev. C 66 (2002) 034614.
[22] W. Luo, et al., GEp-III and GEp2γ Collaborations, Phys. Rev. Lett. 108 (2012) 222004.
[23] M. Sikora, et al., A2 Collaboration at MAMI, Phys. Rev. Lett. 112 (2014) 022501.
[24] S. Strauch, et al., CLAS Collaboration, Phys. Lett. B 750 (2015) 53.
[25] P. Bussey, et al., Nucl. Phys. B 169 (1980) 403.
[26] R. Arndt, et al., Thomas Jefferson Lab, CLAS Approved Experiment E03-105, https://www.jlab.org/exp_prog/abstracts/03/PR03-105.html, 2003.
[27] B.A. Mecking, et al., CLAS Collaboration, Nucl. Instrum. Methods A 503 (2003) 513.
[28] D.I. Sober, et al., Nucl. Instrum. Methods A 440 (2000) 263.
[29] K. Livingston, Jefferson Laboratory, CLAS Note 2011-020, https://misportal.jlab.org/ul/Physics/Hall-B/clas/viewFile.cfm/2011-020.pdf?documentId=656, 2011.
[30] H. Überall, Z. Naturforsch. A 17 (1962) 332.
[31] N. Zachariou, Ph.D. Thesis George Washington University, 2012, https://www.jlab.org/Hall-B/general/thesis/Zachariou_thesis.pdf.
[32] A.M. Sandorfi, S. Hoblit, H. Kamano, T.-S.H. Lee, J. Phys. G 38 (2011) 053001.
[33] C. Keith, et al., Nucl. Instrum. Methods A 684 (2012) 27.
[34] M. Dugger, et al., CLAS Collaboration, Phys. Rev. C 88 (2013) 065203.
[35] W.J. Briscoe, et al., A2 Collaboration at MAMI, Phys. Rev. C 100 (2019) 065205.
[36] D. Drechsel, S.S. Kamalov, L. Tiator, Eur. Phys. J. A 34 (2007) 69.
[37] A.V. Anisovich, V. Burkert, J. Hartmann, E. Klempt, V.A. Nikonov, E. Pasyuk, A.V. Sarantsev, S. Strauch, U. Thoma, Phys. Lett. B 766 (2017) 357.
[38] D. Rönchen, M. Döring, H. Haberzettl, J. Haidenbauer, U.G. Meissner, K. Nakayama, Eur. Phys. J. A 51 (2015) 70.
[39] R.A. Arndt, W.J. Briscoe, I.I. Strakovsky, R.L. Workman, Phys. Rev. C 74 (2006) 045205.
[40] D. Rönchen, M. Döring, H. Haberzettl, J. Haidenbauer, U.G. Meißner, K. Nakayama, Eur. Phys. J. A 51 (2015) 70.